JOURNAL OF MATERIALS SCIENCE 25 (1990) 2573–2584

Microstructures and crystallization of electroless Ni–P deposits

KANG-HEON HUR, JAE-HAN JEONG, DONG NYUNG LEE
Department of Metallurgical Engineering, Seoul National University, Seoul 151-742, Korea

A study has been made of microstructures and crystallization of the electroless Ni–P deposits containing 11.3 to 23.0 at% P obtained from acidic nickel sulphate baths with sodium hypophosphite as a reducing agent by means of differential scanning calorimetry, X-ray diffractometry and hot stage transmission electron microscopy. The deposits containing low phosphorus content of 11.3 at% could be represented as an fcc Ni–P solid solution of 5 to 10 nm microcrystallites, whereas the deposits containing high phosphorus content were amorphous. The crystallization process of amorphous Ni–P solution involved more than one intermediate phases; precrystallized nickel or off-stoichiometric $Ni_3(P, Ni)$ or $Ni_5(P, Ni)_2$ phase in which some phosphorus sites are replaced by nickel atoms. The final equilibrium phases were bct Ni_3P and fcc nickel crystals regardless of phosphorus content. The amorphous phase containing 20 to 22 at% phosphorus was the most stable among the amorphous Ni–P alloys.

1. Introduction

Extensive studies have been made of the Ni–P alloys recently, because they have wide industrial applications owing to their excellent corrosion resistant, wear resistant and non-magnetic properties. Moreover Ni–P alloys are simple and typical metal–metalloid amorphous systems and a thorough study of their crystallization process may shed some light on other more complex systems.

The structure of as-deposited Ni–P alloys has been reported to be either amorphous or microcrystalline [1–5]. In general, it has been found that low phosphorus content alloys are phosphorus-supersaturated solid solutions of crystalline nickel whose lattice becomes more and more strained, and grain sizes decrease with increasing phosphorus concentration. Occasionally, the deposits have been found to have fibre textures with [1 1 1] orientation [4, 5]. The alloys with 12 to 14 wt % P are amorphous. The main features of the interference functions of the Ni–P alloys with high phosphorus content can be depicted by the dense random packing of hard sphere model [6].

Since the solubility of phosphorus in crystalline nickel is very low, the alloys are in a metastable state, the stability of which depends strongly on the composition. Therefore the crystallization mechanism can vary with alloy compositions. The X-ray diffraction, transmission electron microscopy and differential scanning calorimetry studies have reported various mechanisms and intermediate phases for the crystallization of the Ni–P alloys even with the same composition.

Generally, the whole composition range up to 25 at % P can be divided into two regions according to the reported DSC and TEM studies. For the composition of $P < 20$ at %, the crystallization of the amorphous alloys leads to precipitation of fine nickel crystallites and the remaining phosphorus rich matrix is crystallized into the equilibrium phase, Ni_3P crystallines. For phosphorus composition of greater than 20 at %, the first stage crystallization reaction leads to various metastable phases which are subsequently decomposed into final equilibrium phases. The metastable phases have been reported to have different structures and lattice constants [7, 8].

Near the eutectic region (= 20 at % P) where many competing crystallization reactions take place, the reaction path depends very sensitively on composition. Therefore the crystallization behaviour in this region cannot be described by only one mechanism.

The purpose of this work is to study the microstructures and the crystallization behaviour of electroless Ni–P deposits with various phosphorus contents, in particular, near the eutectic composition by transmission electron microscopy, differential scanning calorimetry and X-ray diffractometry.

2. Experimental procedure

2.1. Electroless nickel plating

To prepare electroless nickel deposits, a 5086 aluminium sheet which had been previously zincated was used as substrate, nickel sulphate as a nickel source and sodium hypophosphite as a reducing agent. To study the effect of phosphorus content on the microstructure and phase transformation of electroless Ni–P deposits, deposits with various phosphorus contents were obtained by varying the parameters which determine the phosphorus content in the electroless Ni–P deposits.

The plating solutions used in this study are given in Table I. The phosphorus contents in Ni–P deposits were analysed by emission spectroscopy of direct current plasma. The phosphorus contents in the deposits obtained from the solutions are given in Table II.

0022-2461/90 $03.00 + .12

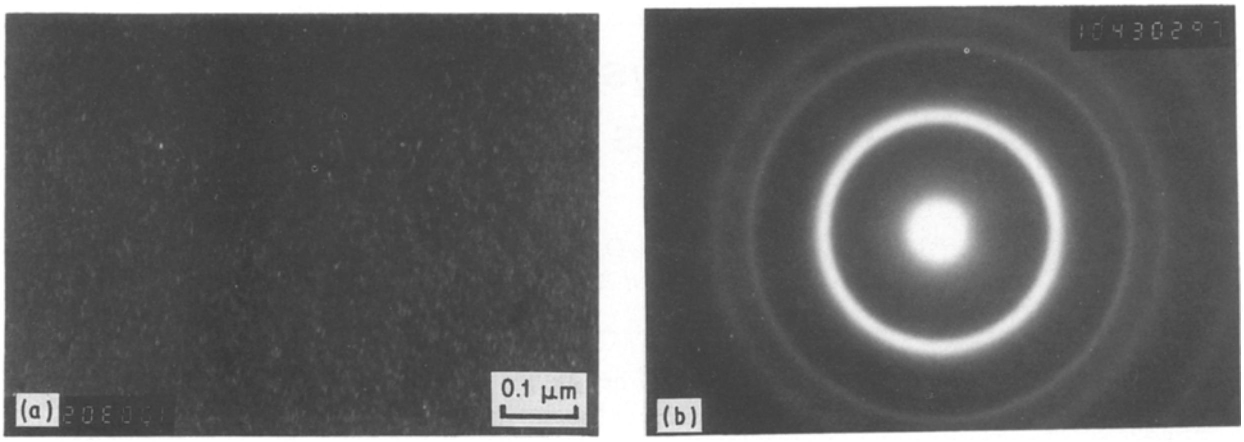

Figure 1 Dark field microstructure and electron diffraction pattern of the as-deposited Ni–P alloy obtained from solution A.

2.2. DSC analysis

The crystallization temperature of the electroless deposits separated from the substrate was measured using a ULVAC DSC 7000 M at a heating rate of $10\,\mathrm{K\,min^{-1}}$.

2.3. TEM analysis

The Ni–P deposits of 10 to $30\,\mu$m thickness which were obtained by electroless plating were separated by dissolving the substrate in 20 % hot sodium hydroxide solution. The separated deposits were cut to 3 mm diameter and thinned by mechanical polishing of both sides of them and finally thinned to a suitable thickness for TEM by twin jet polishing. The electrolyte for twin jet polishing consisted of 10 % perchloric acid, 10% glycerol and 80% methanol cooled to 0° C.

In situ heating experiments were carried out to 600° C in order to observe the crystallization process of the electroless Ni–P deposits. A furnace type heating stage with JEOL EM-SHH heating holder and EM-SHU2 heater control unit were used in this study.

2.4. X-ray diffraction analysis

X-ray diffraction analyses were performed in two ways using a Rigaku X-ray diffractometer unit. To measure intensity for calculation of pair distribution function and radial distribution function a step scanning method was used with Mo Kα radiation. For the step scanning, the step width was 0.2°, and the counting time for one step was 100 sec. To measure the X-ray diffraction patterns of the heat treated deposits the common continuous scanning method was used with Cu Kα radiation. Heat treatment of the deposits was carried out under argon atmosphere in a tube furnace at 200 to 450° C for 2 h.

TABLE I Chemical composition of electroless nickel plating solutions* (*g/l*)

Constituents	Solutions				
	A	B	C†	D	E
$NiSO_4 \cdot 6H_2O$	26.3	26.3		26.3	26.3
$NaH_2PO_2 \cdot H_2O$	10.5	10.5		26.3	26.3
Na-acetate	34.0	34.0	EN422A	34.0	34.0
Latic acid	18.0	18.0	EN422B	18.0	18.0
Malic acid	21.1	21.1		21.1	–
Citric acid	–	–		–	31.5
pH‡	5.5	5.0	4.5	4.5	5.0

*Solution temperature was maintained at 90 ± 1° C.
†EN422A and B is the commercial electroless nickel plating solution for coating of memory disc underlayer.
‡pH was adjusted with NH_4OH.
§Except solution C, lead nitrate 3.2×10^{-3} g/l was used as a stabilizer.

3. Results and discussion

3.1. Structure analysis

Figs 1a and b show the TEM dark field micrograph and electron diffraction pattern of the as-deposited Ni–P alloy obtained from solution A (6.3 wt % P). The diffraction pattern shows a broad inner ring and two sharp outer rings indicating f c c nickel. The dark field image with the objective aperture centred on the (1 1 1) and (2 0 0) rings shows many fine grains (about 5 to 10 nm white grains in Fig. 1a). The grain size of the deposit calculated by the Scherrer formula, based on line broadening of X-ray diffraction peak, was about 5 nm which is comparable with the value observed in TEM microstructure, taking into account the residual stress developed in the specimens during plating. The TEM microstructure and electron diffraction pattern of the as-deposited Ni–P alloy obtained from solution C (11.5 wt % P) indicate typical amorphous characteristics (Fig. 2). The TEM microstructures and electron diffraction pattern of the electroless Ni–P deposits obtained from the other solutions were similar to ones of the sample obtained from solution C.

To scrutinize the microstructures of the as-deposited Ni–P alloys with various phosphorus contents, we calculated the pair distribution functions (Fig. 3) and radial distribution functions (Fig. 4) from X-ray diffraction results. The pair distribution function of the

TABLE II Content of phosphorus in electroless nickel deposits obtained from various solutions

Solutions	P (wt %)	P (at %)	Ni_3P* (wt %)	Ni_3P (vol %)
A	6.3	11.3	42.1	45.3
B	10.1	17.5	67.5	70.3
C	11.5	19.8	76.9	79.1
D	12.5	21.3	83.6	84.2
E	13.6	23.0	90.9	91.9

*The Ni_3P content was calculated assuming that all phosphorus forms Ni_3P when annealed.

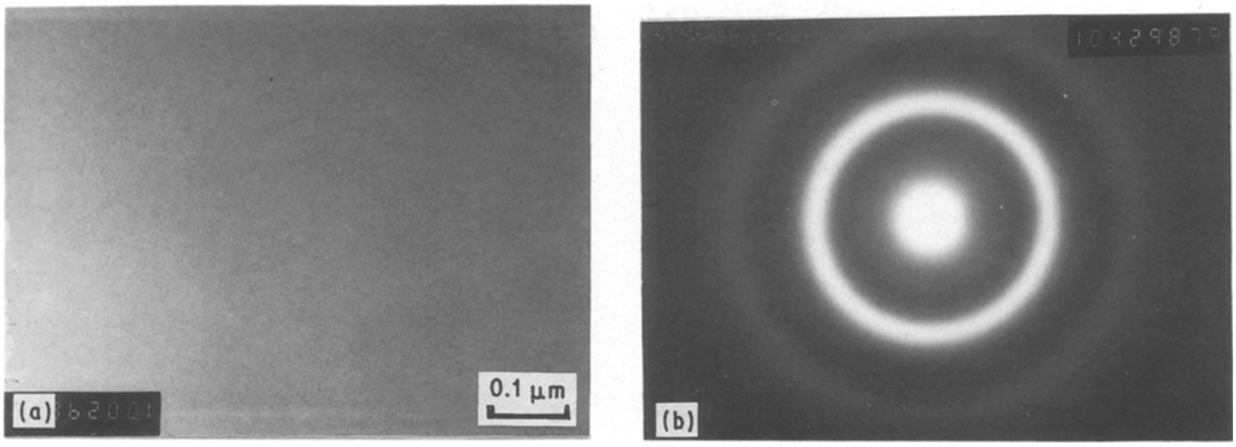

Figure 2 TEM microstructure and electron diffraction pattern of the as-deposited Ni–P alloy obtained from solution C.

as-deposited Ni–P alloys obtained from solution A indicates that crystalline characteristics were maintained above 1.6 nm from the centre atom. The pair distribution function of the as-deposited Ni–P alloys obtained from solution C shows the splitting of the second peak and approaches unity at large values of r (above 1 nm) which are amorphous characteristics. The Ni–P deposits obtained from the other solutions were similar to the deposit obtained from solution C. The distance from the origin to the first maximum peak in the radial distribution function indicates the average nearest-neighbour atom distance. The average nearest-neighbour atom distance of sample (11.3 at %) obtained from solution A were calculated to be 0.246 nm and those from the others were calculated to be 0.253 to 0.256 nm with increasing phosphorus content.

The nearest-neighbour atom distance calculated using Vegard's law on the assumption that the solution A deposit was phosphorus-supersaturated solid-solution of crystalline nickel is 0.246 nm. The value is in very good agreement with that calculated from the radial distribution function. However the average nearest-neighbour atom distances of samples obtained from the other solutions B, C, D and E were larger than the diameter of nickel atom, 0.249 nm, even though they contained higher phosphorus than that from solution A (the diameter of phosphorus atom is 0.218 nm). The results are in contradiction to Vegard's law. All the results suggest that the deposit with lower phosphorus contents was phosphorus-supersaturated crystalline nickel and the deposits with higher phosphorus contents were amorphous.

3.2. Crystallization

3.2.1. Differential scanning calorimetry and X-ray diffraction analyses

Fig. 5 shows the results of thermal analysis using a DSC at 10 K min^{-1} heating rate for Ni–P specimens of various phosphorus contents, indicating that the amorphous (or microcrystalline)-to-crystalline transformation are exothermic. The amorphous samples shows two transformation peaks, both of which are simple and well defined. The appearance of more than two transformation peaks may be considered to be a phenomenon caused by a large difference in phosphorus concentration along the thickness of the layer or by some other structural inhomogeneity. The DSC results will be explained with reference to the X-ray diffraction results of the Ni–P deposits annealed at various temperatures for 2 h. The sample obtained from the solution A shows only a small DSC peak at about 400° C (Fig. 5a). This peak is caused by the crystallization of the supersaturated microcrystalline

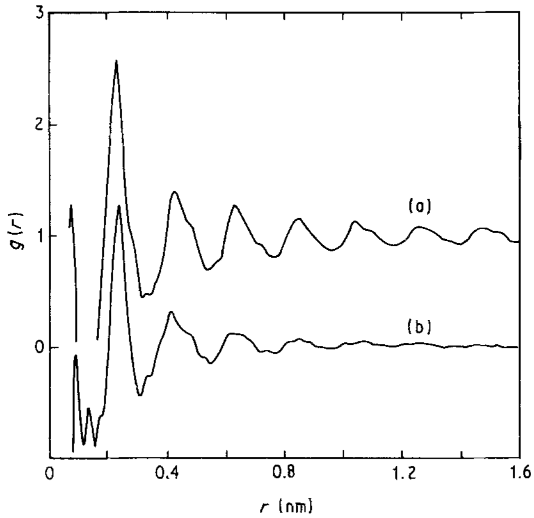

Figure 3 Pair distribution functions of electroless Ni–P alloys obtained from (a) solution A, and (b) solution C.

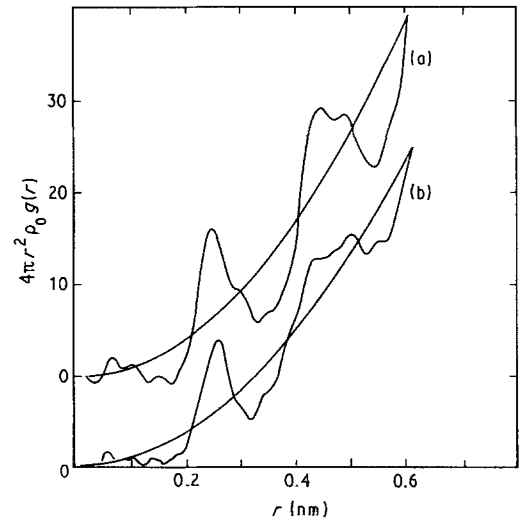

Figure 4 Radial distribution functions of electroless Ni–P alloys obtained from (a) solution A, and (b) solution C.

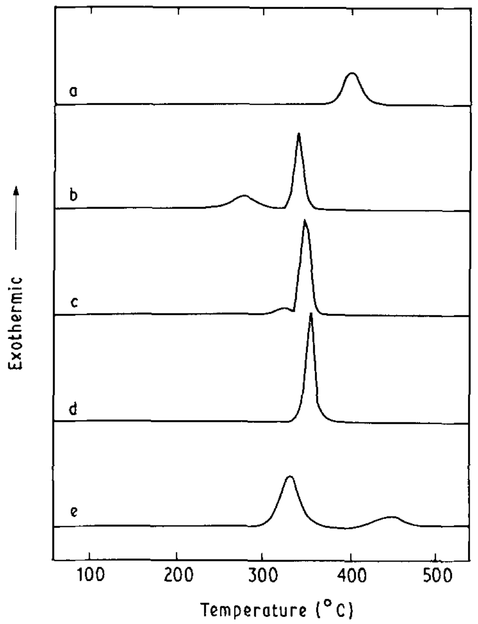

Figure 5 Differential scanning calorimetry curves of the crystallization processes for the electroless nickel deposits obtained from various solutions. (a) Solution A, (b) solution B, (c) solution C, (d) solution D and (e) solution E.

to Ni_3P phase. The sample obtained from solution B shows a very well defined DSC peak at 340° C preceded by a broad peak ranging from 200 to 300° C (Fig. 5b). According to the X-ray diffraction analysis (Fig. 6b), the first broad and shallow peak represents the fcc nickel crystallites precipitated in amorphous matrix. The second sharp peak indicates decomposition of the remaining phosphorus-rich amorphous matrix into Ni_3P crystallites and nickel crystallites.

The deposit obtained from the solution C showed a very weak DSC peak at about 320° C, followed by a sharp peak at 350° C. The X-ray diffraction analysis indicated that these two reactions resulted in formation of nickel and Ni_3P crystallites. The sample obtained from solution D gave us only a sharp peak at 355° C that is thought to occur due to the direct (polymorphous) crystallization of amorphous to $Ni_3(P, Ni)$ crystalline which implies that the phosphorus lattice sites are occupied by phosphorus and nickel atoms.

The sample obtained from the solution E also gave rise to two exothermic effects, that is, the first sharp DSC peak at about 335° C and the second much weaker and broader peak between 400 and 480° C. The X-ray diffraction pattern of the sample annealed at 350° C showed the crystallization into the metastable phase indexed as Ni_5P_2 crystallite (Fig. 6e), but did not include any other crystallite phases. The other weak exothermic peak is thought to be associated with decomposition of the metastable Ni_5P_2 crystallites into nickel crystallites and equilibrium phase Ni_3P crystallites. The X-ray diffraction pattern of the deposit annealed at 450° C showed only nickel and Ni_3P crystalline peaks and the diffraction peaks of Ni_5P_2 phase were not found (Fig. 6e).

The temperatures of exothermic peaks in the DSC curves mentioned above for electroless Ni–P deposits are shown as a function of phosphorus contents in Fig. 7. For comparison comprehensive literature data

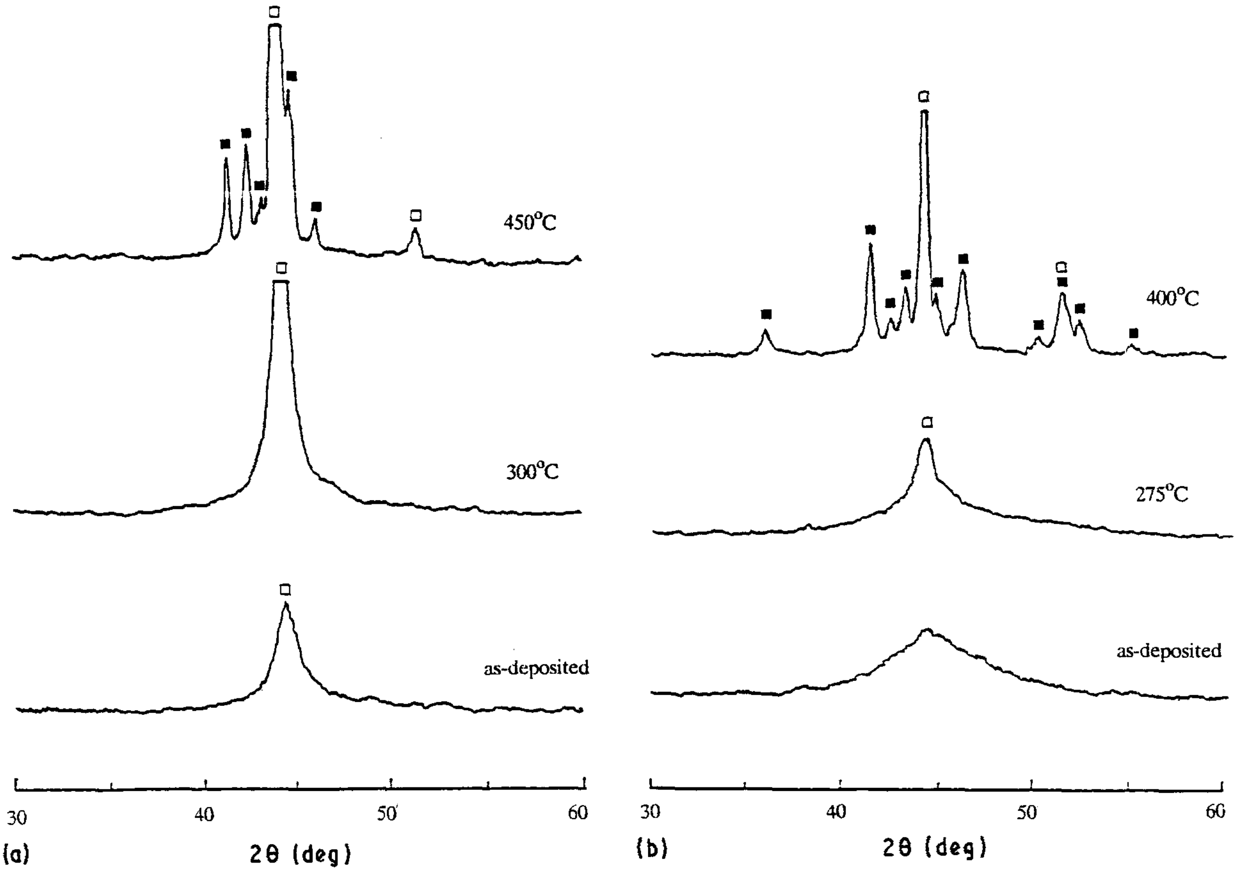

Figure 6 X-ray diffraction patterns of the electroless Ni–P alloys obtained from the various solutions (□ Ni, ■ Ni_3P, ● Ni_5P_2). Annealing was performed at the various temperatures for 2 h. (a) solution A, (b) solution B, (c) solution C, (d) solution D and (e) solution E.

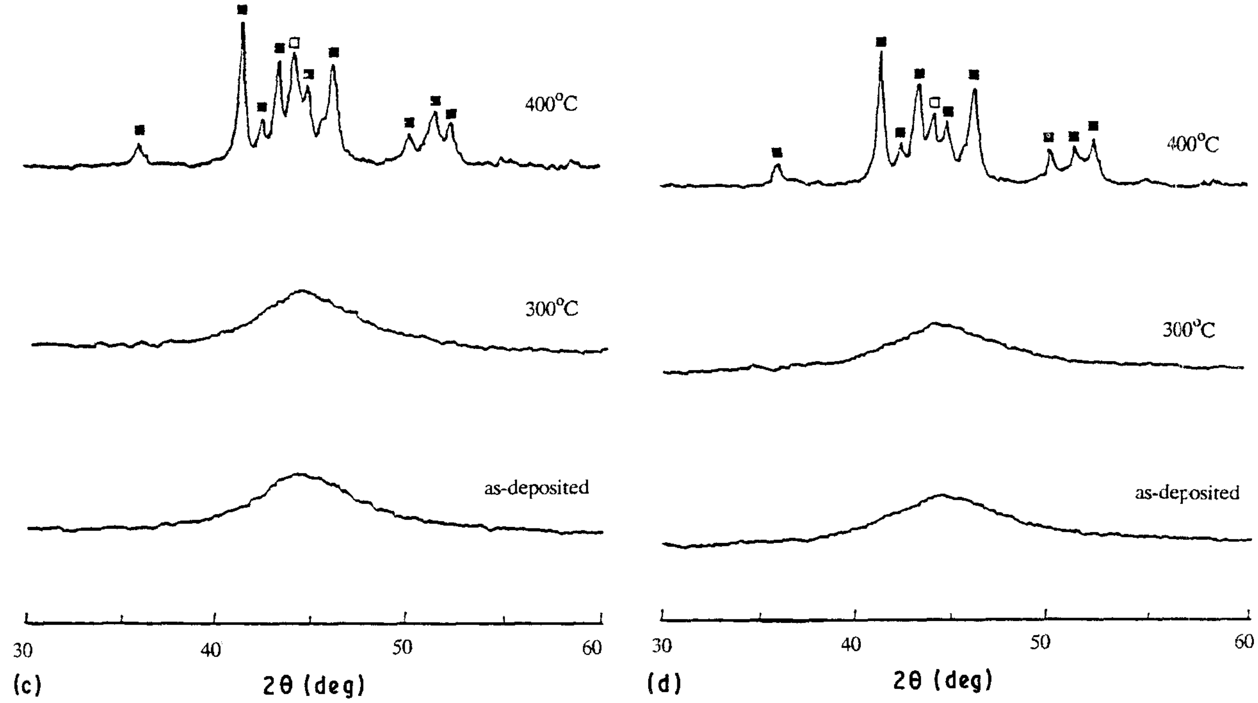

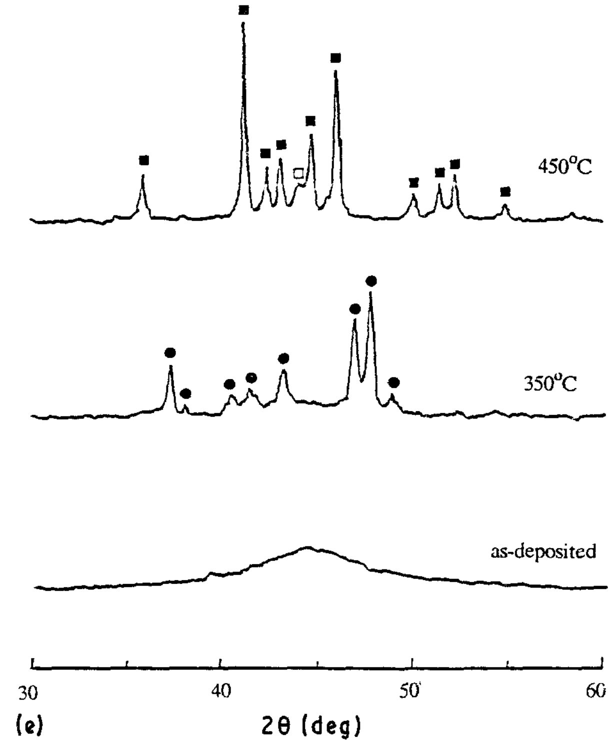

Figure 6 Continued

from DSC analysis on electrodeposited Ni–P alloys are added [3, 9–13]. The present results are similar to the general trend obtained from electrodeposited Ni–P alloys. The above discussion will be augmented by the following hot stage TEM observation.

3.2.2. Hot stage TEM analysis

Fig. 8 shows TEM microstructures and electron diffraction patterns of solution A deposits in various heating stages. On heating to 300° C grain coarsening occurred (Fig. 8a), and the diffraction rings corresponding to f c c nickel crystallites became sharper and the inner ring was separated into (1 1 1) and (2 0 0) rings. The diffraction pattern of Ni_3P phase is, however, not shown (Fig. 8b). On heating the deposit further to 350° C, the diffraction spots corresponding to Ni_3P crystallites (tetragonal, $a = 0.895$ nm, $c = 0.439$ nm) appeared together with much sharper diffraction rings of nickel (Fig. 8c). The fact that the spot pattern appeared indicates the Ni_3P crystallite have already grown up large. The shape of Ni_3P grain is, however, indistinct. The result suggests that in the early stage pre-existing f c c nickel grains coarsened, and on further heating, the Ni_3P crystallites nucleated in the phosphorus rich matrix and grew rapidly by encircling nickel grains. On further heating to 450° C nickel grains grew up to about 50 nm and the diffraction ring became spot pattern (Figs 8e and f).

The microstructures and electron diffraction patterns of the solution B deposit in various heating stages are shown in Fig. 9. Very fine nickel precipitates

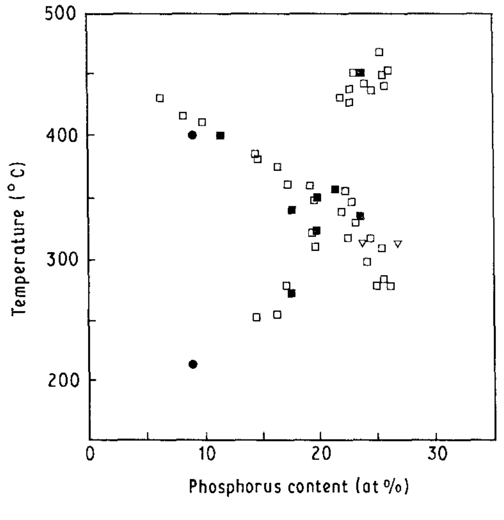

Figure 7 The temperatures of exothermic peaks in the DSC curves for electroless and electro Ni–P deposits as a function of phosphorus content. (□ [3, 9, 10, 11], 20 K min^{-1}; ▽ [12], 20 K min^{-1}; ● [13], 20 K min^{-1}; ■ present work, 10 K min^{-1}).

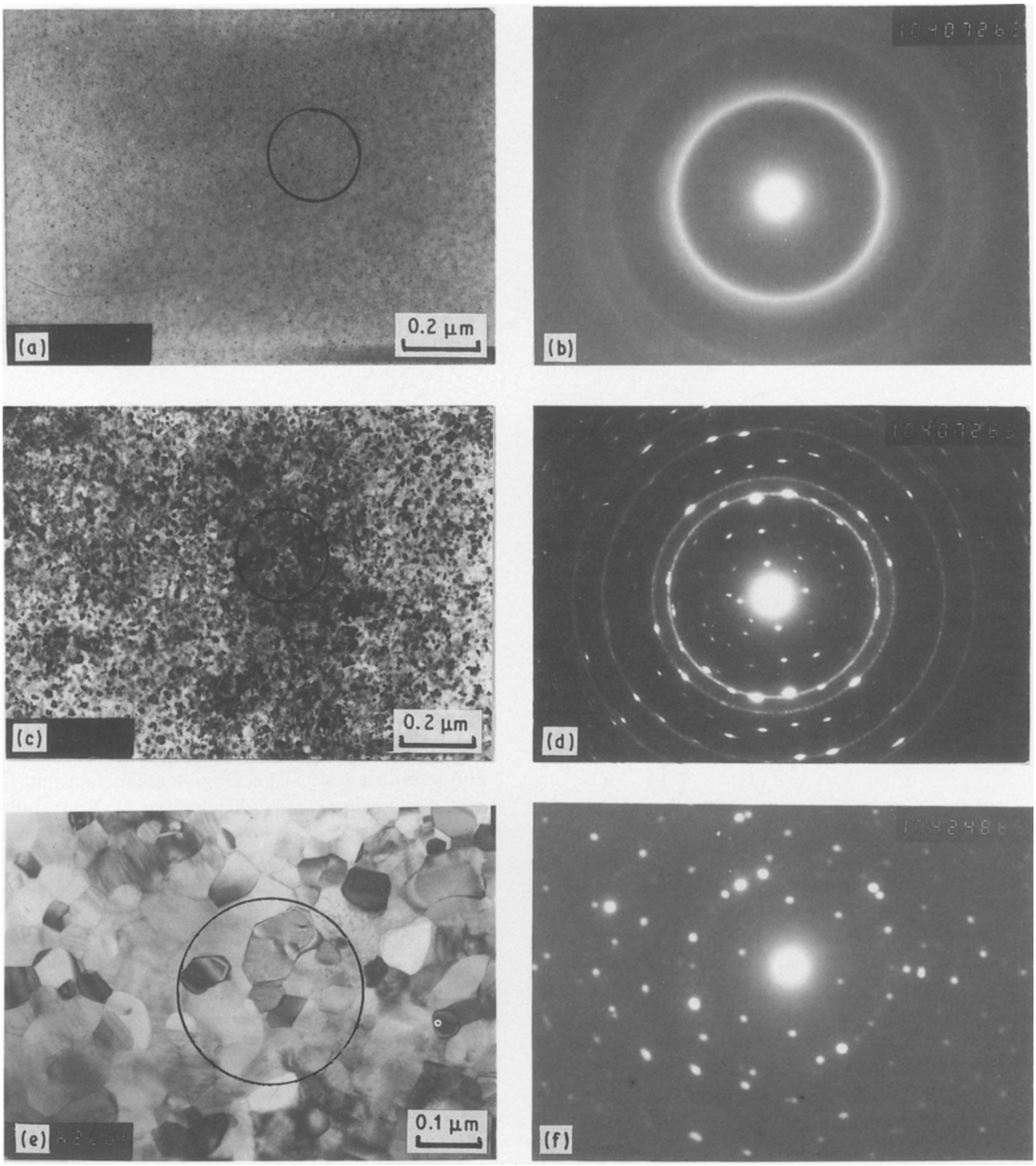

Figure 8 Transmission electron microstructures and electron diffraction patterns of the electroless Ni–P alloy obtained from solution A in various hot stages. (a) and (b) 300° C; (c) and (d) 350° C; (e) and (f) 450° C.

(black dots) appeared in amorphous matrix at 250° C (Fig. 9a). The inner broad diffused rings in the electron diffraction pattern in Fig. 9b is from the amorphous matrix, and the outer sharp rings are the reflections of the crystalline nickel particles precipitated out. Heating to 310° C produced the microstructure shown in Fig. 9c. Here the transformation of amorphous matrix to crystalline Ni_3P is shown to have proceeded with the formation of spherical spherulites. The fine dispersions of nickel crystallites already precipitated are shown in the crystalline Ni_3P. This is confirmed by the electron diffraction pattern, in which the continuous spot rings originate from the fine nickel particles and the spot pattern which have streaks is from the large spherulitic Ni_3P grain (Fig. 9d). The electron diffraction pattern indicates that the spherulitic morphology is a single crystal or a single crystal containing subgrains of small misorientation which grow radially from the centre. The streak pattern seems to originate from the small misorientation. On further heating, the spherulitic Ni_3P grains grew until they impinge on one another (Fig. 9e). Heating the sample to 550° C gave rise to loss of the radial spherulitic Ni_3P morphology and coarsening of the nickel particles in Ni_3P grains or grain boundaries (Fig. 9f). The streak disappeared in the electron diffraction pattern of Ni_3P phase (Fig. 9g).

The microstructures and electron diffraction patterns of the solution C deposits in hot stages at 330° C are shown in Fig. 10. Fig. 10a shows the precrystallized

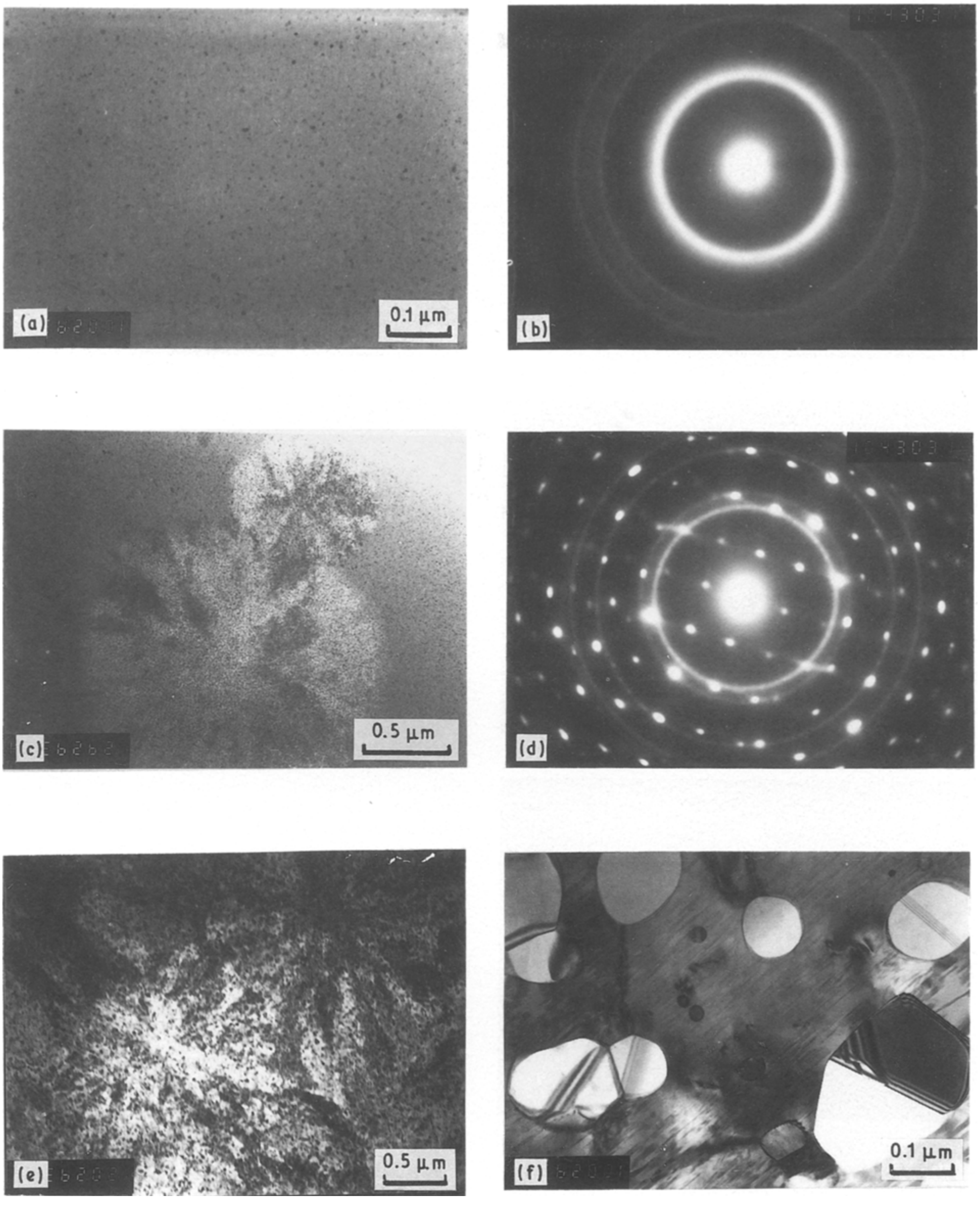

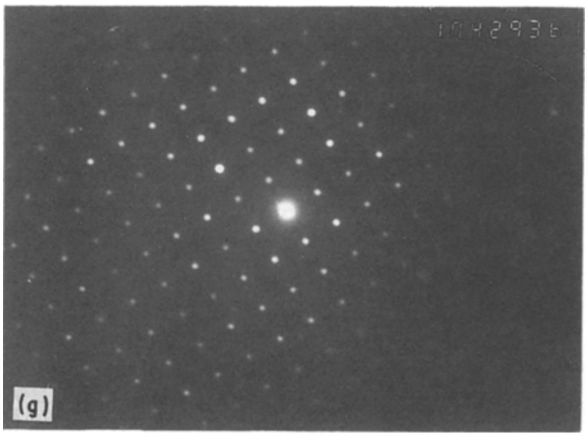

Figure 9 Transmission electron microstructures and electron diffraction patterns of the electroless Ni–P alloy obtained from solution B in various hot stages. (a) and (b) 250° C; (c) and (d) 310° C; (e) 360° C; (f) and (g) 550° C.

nickel crystallites (region A) and the ellipsoidal Ni_3P spherulites including relatively coarse precrystallized nickel crystallites and very fine nickel particles (region B). Electron diffraction patterns of the two regions A and B are shown in Figs 10b and c. The major part of the film was subjected to the above crystallization process, while there were some regions which crystallize into spherulitic Ni_3P (including very fine nickel

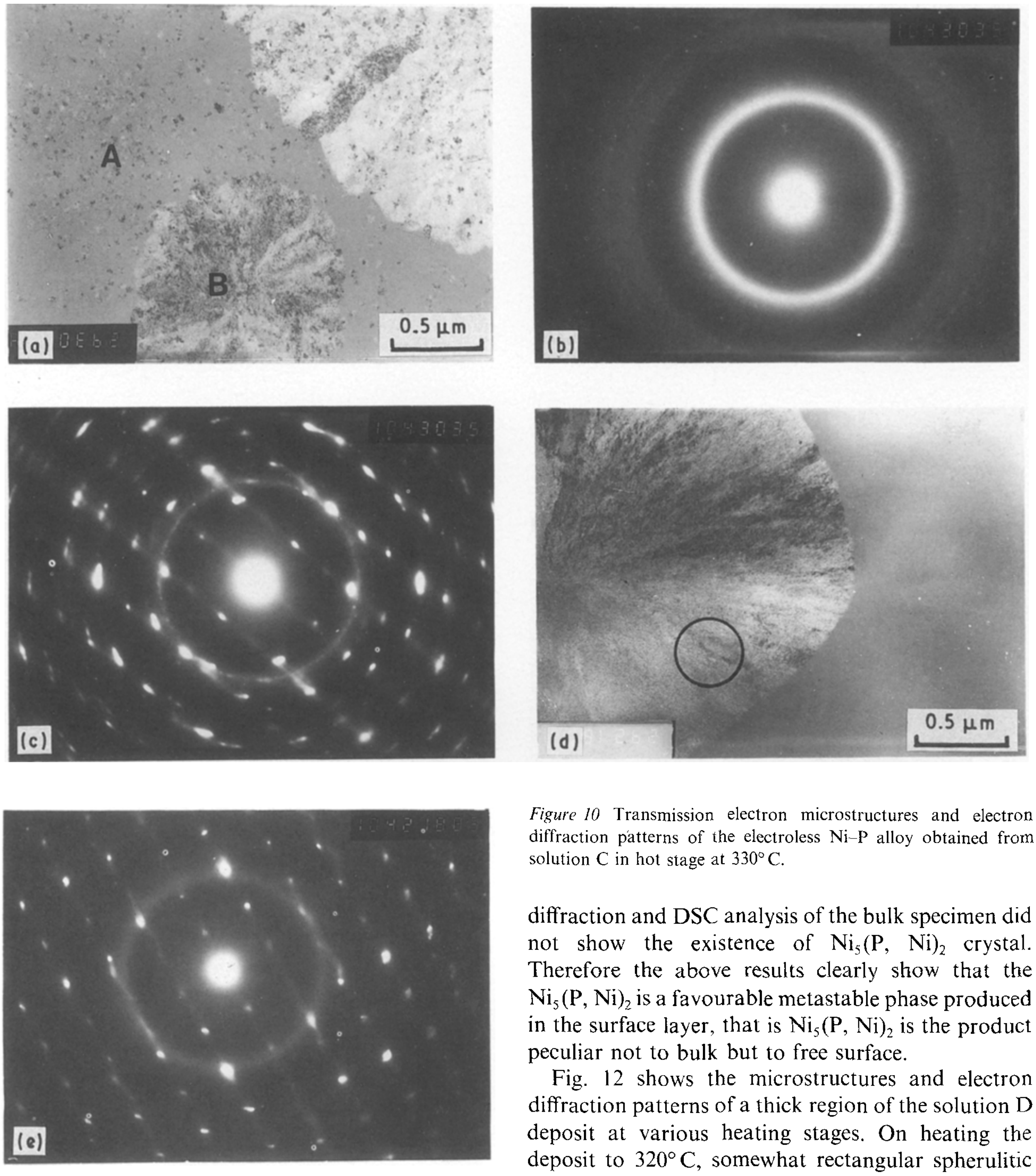

Figure 10 Transmission electron microstructures and electron diffraction patterns of the electroless Ni–P alloy obtained from solution C in hot stage at 330° C.

particles) without any precrystallized nickel grains in the amorphous matrix (Figs 10d and e). The subsequent crystallization behaviour is very similar to that of the deposits obtained from solution B.

Fig. 11 shows the microstructures and electron diffraction patterns in thin region of the solution D deposit at 280° C. Cigar-like or feather-like crystals including many fine particles were nucleated at the edge of the film (Figs 11a and b). The electron diffraction pattern of the crystals indicated that the crystals were $Ni_5(P, Ni)_2$ phase (hexagonal, $a = 1.322\,nm$, $c = 2.463\,nm$) and the fine particles were nickel crystallites rejected from $Ni_5(P, Ni)_2$ phase due to the limited solubility of nickel to $Ni_5(P, Ni)_2$ phase (Fig. 11c). The $Ni_5(P, Ni)_2$ crystals were not found in thick regions, the major part of the film, but in thin regions of the film. The $Ni_5(P, Ni)_2$ phase decomposed into Ni_3P phase and nickel later. The results of X-ray diffraction and DSC analysis of the bulk specimen did not show the existence of $Ni_5(P, Ni)_2$ crystal. Therefore the above results clearly show that the $Ni_5(P, Ni)_2$ is a favourable metastable phase produced in the surface layer, that is $Ni_5(P, Ni)_2$ is the product peculiar not to bulk but to free surface.

Fig. 12 shows the microstructures and electron diffraction patterns of a thick region of the solution D deposit at various heating stages. On heating the deposit to 320° C, somewhat rectangular spherulitic $Ni_3(P, Ni)$ crystals were nucleated randomly in the thick region of film. Fig. 12a shows the $Ni_3(P, Ni)$ spherulite (region A) co-existing with the $Ni_5(P, Ni)_2$ grain. Electron diffraction pattern of the spherulitic crystal showed streak spot pattern indexed as Ni_3P phase, but did not show nickel reflections (Fig. 12b). The absence of nickel reflections in Fig. 12b is probably due to dissolving of nickel into the lattice of the $Ni_3(P, Ni)$ and a very small amount of crystallized nickel particles in the $Ni_3(P, Ni)$ matrix, if any. Fig. 12c represents a dark field image showing the absence of nickel particles, but locally the spherulitic Ni_3P crystals including many fine nickel particles were found (Figs 12d and e). One reasonable explanation for the latter phenomenon could be rejection of excess nickel which could not be dissolved due to its limited solubility to $Ni_3(P, Ni)$ phase in some nickel rich regions. Fig. 12f shows the completion of spherulitic Ni_3P crystallization. The nickel particles are not

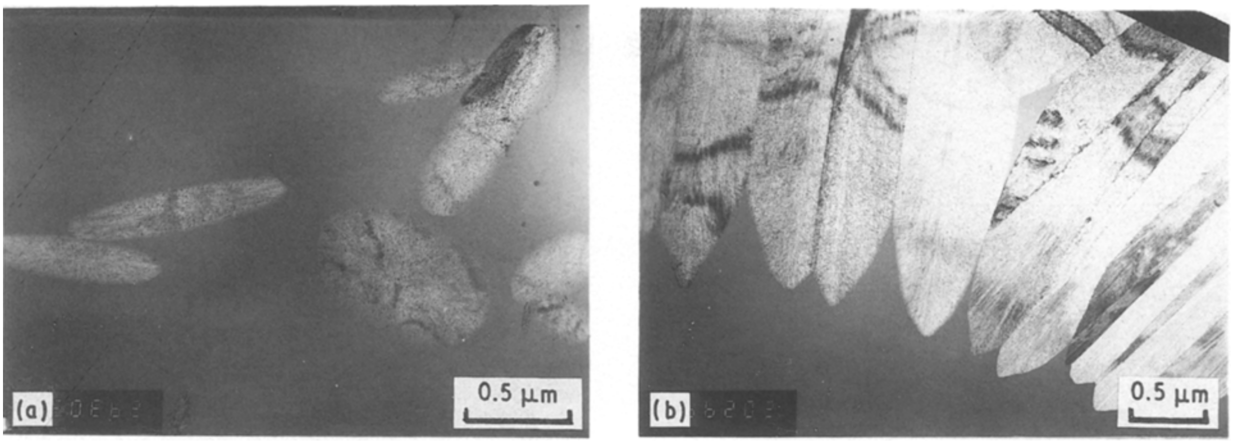

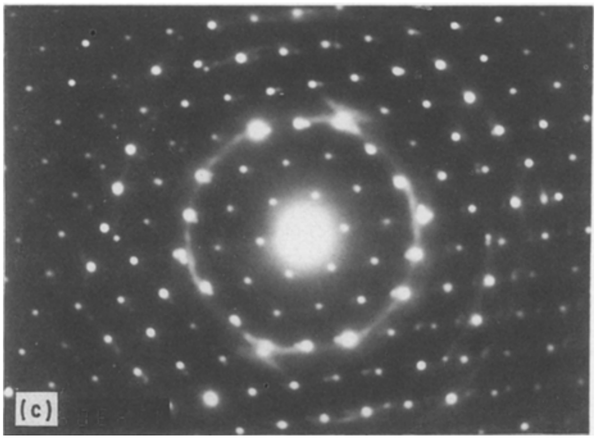

Figure 11 Transmission electron microstructures and electron diffraction patterns of a thin region of the electroless Ni–P alloys obtained from solution D at hot stage of 280° C.

shown clearly yet. On heating to 420° C, nickel particles radially precipitated in $Ni_3(P,Ni)$ coarsened (Fig. 12g). The nickel diffraction rings now appeared in the electron diffraction pattern. The subsequent crystallization behaviour is very similar to those of the solution B and C deposits (Fig. 12h).

The microstructures and electron diffraction patterns of the solution E deposits at various heating temperatures are shown in Fig. 13. On heating to 270° C in the hot stage, dendritic morphologies were found, first at the edge and then growing toward the interior of the film, as shown in Fig. 13a. The individual dendrites were several micrometres long and the secondary arms of the dendrites were at about 90° to the stem in some cases and 60° in others. One possible explanation for the formation of these dendrites within the amorphous matrix could be that it might be due to the high thermal conductivity of the region where the concentration ratio of nickel to phosphorus atoms is the highest. The high nickel region was formed as a result of the rejection of nickel atoms from $Ni_5(P, Ni)_2$ crystals to amorphous ahead of the crystallization front. This dendritic morphology was reported by Bagley *et al.* [13], in their flash evaporated Ni–24.9 at % P alloys and Makhsoos [14] in his electrodeposited Ni–22 at % P deposits.

Fig. 13b shows the electron diffraction pattern of the film of Fig. 13a which conforms to the reflection of the basal plane of the Ni_5P_2 crystalline. The absence of nickel reflection in the electron diffraction pattern indicates that Ni_5P_2 crystallites are off-stoichiometric in which lattice nickel atoms are dissolved. Fig. 13c shows the complete crystallization to $Ni_5(P, Ni)_2$ crystallites. The columnar structure was formed by the impingement of dendrites and nickel atom rejected due to the limited solubility into $Ni_5(P, Ni)_2$ precipitated at grain boundaries. Heating of the film to 450° C resulted in the decomposition of $Ni_5(P, Ni)_2$ into nickel crystallites and Ni_3P crystallites (Fig. 13d). The dark field image (Fig. 13e) shows the interface between the $Ni_5(P, Ni)_2$ (region A) and Ni_3P (region B) crystallite regions. The small white particles in the Ni_3P region are nickel grains. The electron diffraction pattern of regions A and B are shown in Figs 13f and g. Fig. 13h is the microstructure of the film at 550° C showing well defined Ni_3P grains and intergranular growth of nickel particles.

On the basis of the results of DSC analysis, X-ray diffraction and hot stage TEM analysis, a schematic drawing of hypothetical free energy against composition diagram for the phases involved in the electroless Ni–P alloys can be constructed as in Fig. 14.

The observed reactions indicated by arrows are as follows

Deposits A : $\text{Ni–P (s.s)} \xrightarrow{(1)} \text{Ni} + \text{Am.}' \xrightarrow{(1)'} \text{Ni} + Ni_3P$

Deposits B : $\text{Ni–P (Am.)} \xrightarrow{(2)} \text{Ni}^0 + \text{Am.}'$

$\xrightarrow{(2)'} \text{Ni}^0 + (\text{Ni}' + Ni_3(P, Ni))$

$\xrightarrow{(2)''} \text{Ni}^0 + (\text{Ni} + Ni_3P)$

Deposits C : $\text{Ni–P (Am.)} \xrightarrow{(3)} \text{Ni}^0 + \text{Am.}'$

$\xrightarrow{(3)'} \text{Ni}^0 + (\text{Ni}' + Ni_3(P, Ni))$

$\xrightarrow{(3)''} \text{Ni}^0 + (\text{Ni} + Ni_3P)$

Deposits C or D (locally) : Ni-P (Am.)

$\xrightarrow{(4)} \text{Ni}' + Ni_3(P, Ni)$

$\xrightarrow{(4)'} \text{Ni} + Ni_3P$

Deposits D : $\text{Ni-P (Am.)} \xrightarrow{(5)} Ni_3(P, Ni)$

$\xrightarrow{(5)'} \text{Ni} + Ni_3P$

Deposits E : $\text{Ni-P (Am.)} \xrightarrow{(6)} Ni_5(P, Ni)_2$

$\xrightarrow{(6)'} \text{Ni} + Ni_3P$

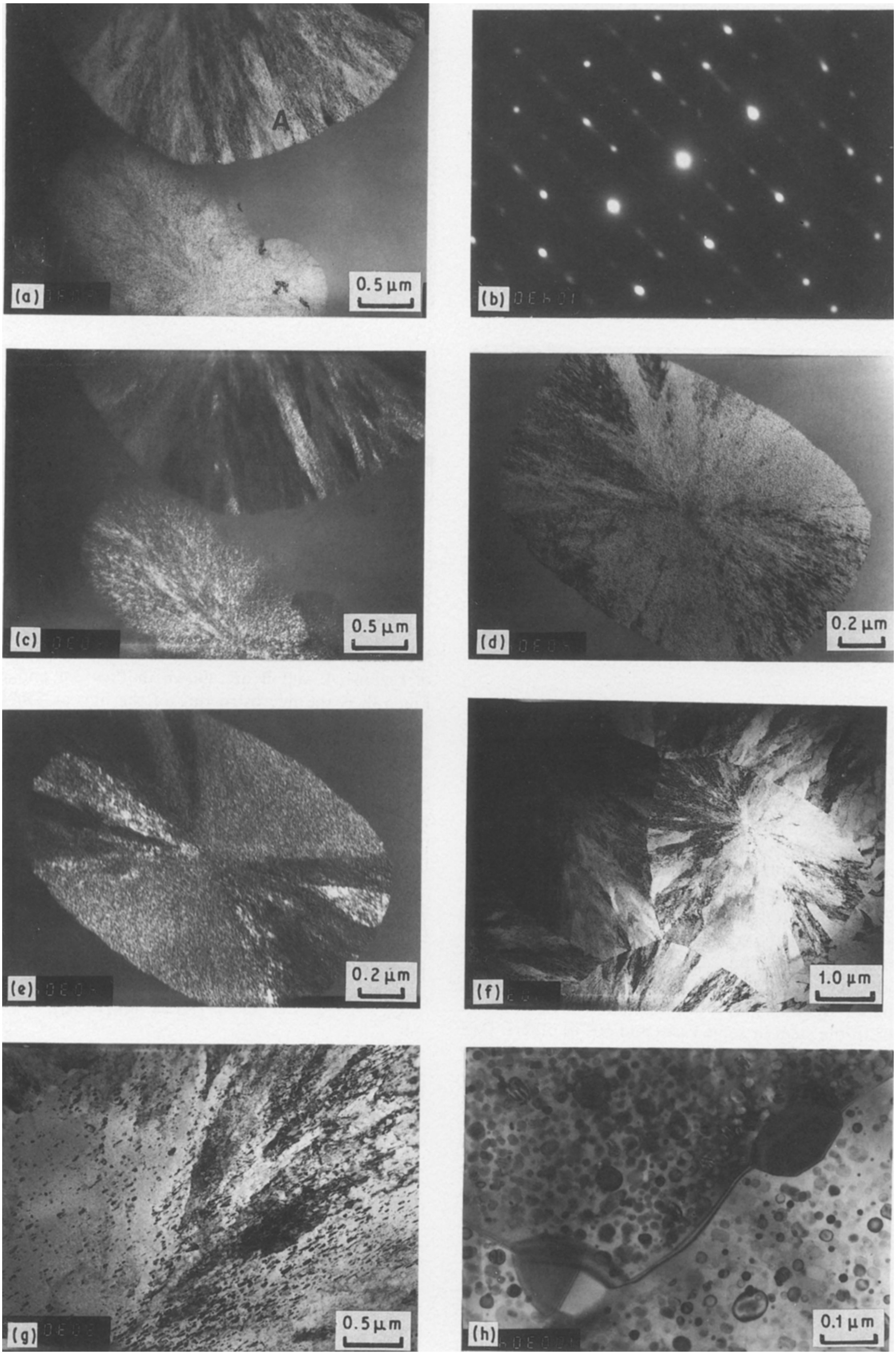

Figure 12 Transmission electron microstructures and electron diffraction patterns of a thick region of the electroless Ni–P alloys obtained from solution D at various hot stages. (a), (b) and (c) 320° C; (d) and (e) 320° C; (f) 365° C; (g) 420° C; (h) 550° C.

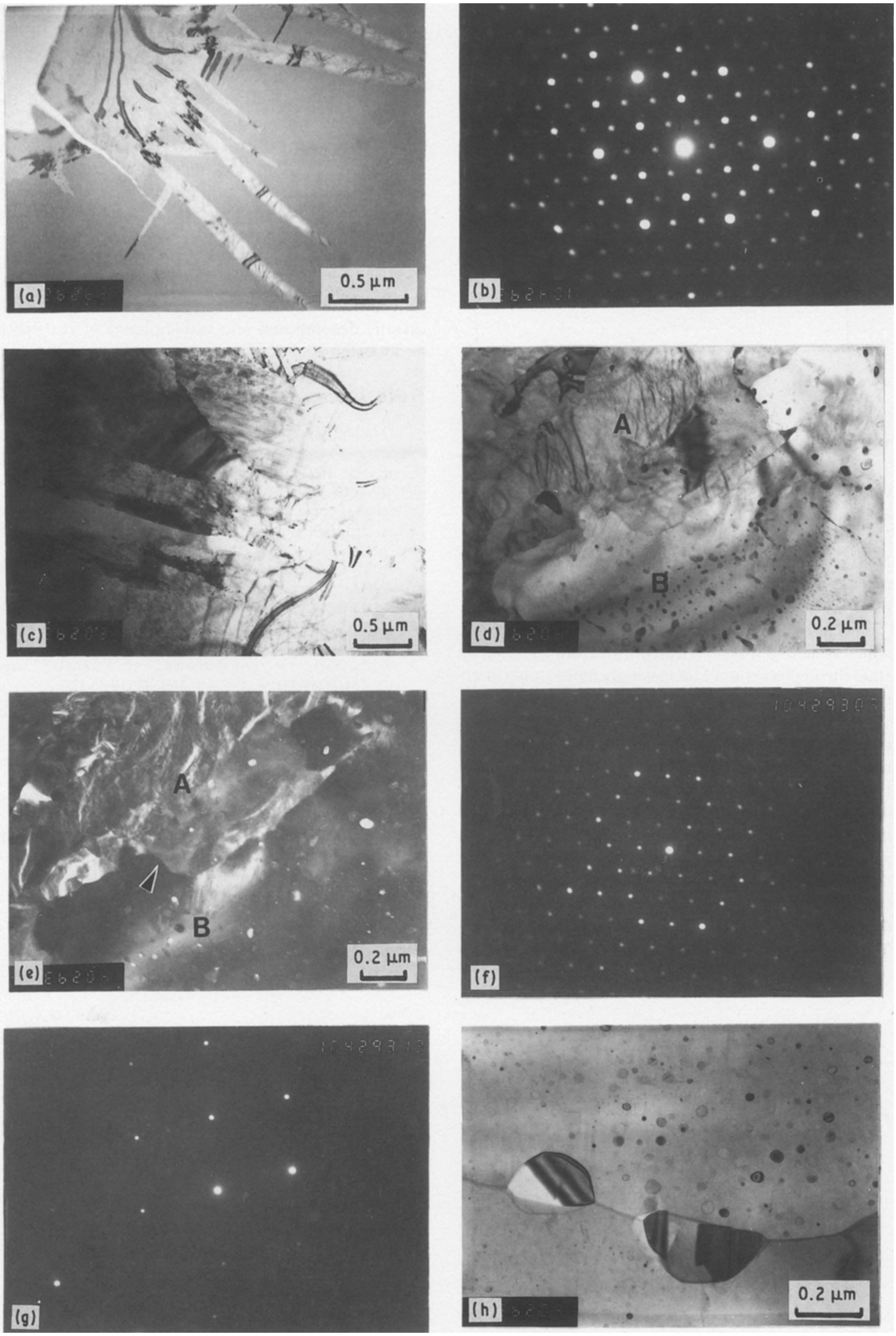

Figure 13 Transmission electron microstructures and electron diffraction patterns of the electroless Ni–P alloys obtained from solution E at various hot stages. (a) and (b) 270° C; (c) 330° C; (d), (e), (f) and (g) 450° C; (h) 550° C.

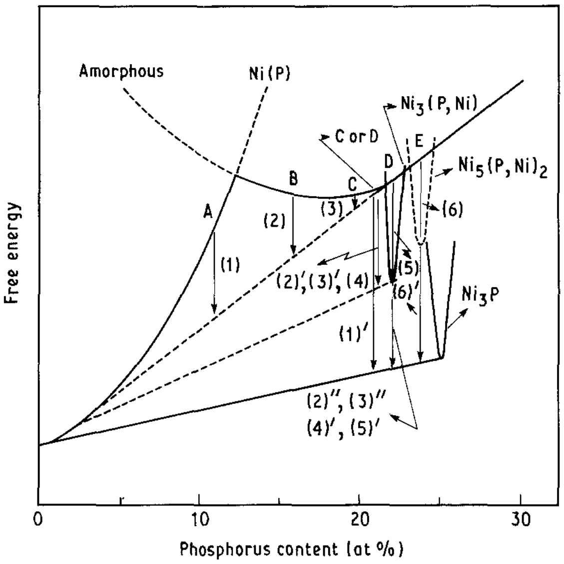

Figure 14 Schematic drawing of hypothetical free energy against composition diagram.

where Ni^0 is precrystallized nickel, Am′ phosphorus enriched amorphous, Ni′ nickel rejected from Ni$_3$(P, Ni) due to its limited solubility into Ni$_3$P, Ni$_3$(P, Ni) and Ni$_5$(P, Ni)$_2$ are off-stoichiometric phases in which phosphorus and nickel atoms share phosphorus sites.

The above reactions obey the Ostwald rule [15], which state that a system transforms from a less stable state through a series of increasingly more stable intermediates to reach the final equilibrium state.

Our results show that the eutectic crystallization, direct crystallization of amorphous into a mixture of nickel and Ni$_3$P phase, did not take place. Also the crystallization behaviour of electroless Ni–P deposits containing the various phosphorus contents lead us to the conclusion that the most stable amorphous phase against any changes in the structure of the alloy is in the range of 20 to 22 at % phosphorus.

4. Conclusions

The electroless Ni–P deposit containing low phosphorus content of 11.3 at % was a phosphorus-supersaturated crystalline nickel solid solution, whose grain size was thought to be 5 to 10 nm. The deposit was decomposed into Ni$_3$P and phosphorus depleted nickel crystallites and subsequent coarsening of the nickel grains when annealed.

The electroless Ni–P deposits containing high phosphorus content had an amorphous structure. The amorphous deposits containing up to 21 at % P crystallized into the spherulitic Ni$_3$(P, Ni) phase preceded by the precrystallized nickel. The amorphous deposits containing phosphorus higher than 21 at % were polymorphically crystallized into metastable phase of bct Ni$_3$(P, Ni) or hexagonal Ni$_5$(P, Ni)$_2$ which was subsequently decomposed into stable phases of fcc nickel and bct Ni$_3$P.

References

1. A. W. GOLDSTEIN, W. ROSTOKER and J. REZEK, *J. Electrochem. Soc.* **119** (1972) 1614.
2. E. VAFAEI-MAKHSOOS, E. L. THOMAS and L. E. TOTH, *Metall. Trans.* **9A** (1978) 1449.
3. K. MASUI, S. MARUNO and T. YAMADA, *J. Jpn Inst. Met.* **41** (1977) 1130.
4. A. H. GRAHAM, R. W. LINDSAY and H. J. READ, *J. Electrochem. Soc.* **112** (1965) 401.
5. S. H. PARK and D. N. LEE, *J. Mater. Sci.* **23** (1988) 1643.
6. J. DIXMIER, *J. Physique* **35** (1974) C4.
7. E. VAFAEI-MAKHSOOS, *J. Appl. Phys.* **51** (1980) 6366.
8. K. H. KUO, *Phil. Mag.* **A51** (1985) 205.
9. K. MASUI, M. TACHIHARA, T. YAMADA and T. TSUJIMOTO, *J. Jpn Inst. Met.* **44** (1980) 124.
10. K. MASUI, T. YAMADA and Y. HISAMATSU, *Kinzoku Hyomen Gijutsu (Japan)* **31** (1980) 667.
11. T. KEMÈNY, B. FOGARASSY and E. TÔTH-KÅDÅR, in Proceedings 3rd International Conference on Soft Magnetic Materials Part 1, Bratislava, 1977.
12. K. MUKASA and MAEDA, *Phys. Status Solidi a* **57** (1980) K93.
13. B. G. BAGLEY and D. TURNBULL, *Acta Metall.* **16** (1970) 857.
14. E. VAFAEI-MAKHSOOS, *J. Mater. Sci.* **16** (1981) 2103.
15. W. OSTWALD, *Z. Phys. Chem.* **22** (1987) 289.

Received 8 February
and accepted 24 August 1989